Bond Behaviour of Oil Palm Broom Fibres in Concrete for Eco-friendly Construction

Author 1
Momoh, Emmanuel Owoichoechi
MSc(ENG), MSc, REng (COREN), MNSE, MNICE, AFHEA
r01eom18@abdn.ac.uk
https://orcid.org/0000-0003-3432-1366

Author 2
*Osofero, Adelaja Israel
PhD (DIC), CEng MICE, FHEA
aiosofero@abdn.ac.uk
https://orcid.org/0000-0002-5476-5979

Author 3
Menshykov, Oleksandr
CSc (PhD), DSc, FHEA
o.menshykov@abdn.ac.uk
https://orcid.org/0000-0003-2869-3307

(All authors)
School of Engineering, University of Aberdeen, King's College, Aberdeen, AB24 3UE, United Kingdom

*Corresponding Author: Osofero, Adelaja Israel
Room 265, Fraser Noble Building,
School of Engineering,
University of Aberdeen,
King's College, Aberdeen,
United Kingdom.
+44 (0)1224 274255
aiosofero@abdn.ac.uk

Abstract

Global awareness towards climate changes and sustainability has attracted research into the use of natural materials in construction. Recent studies on the ribs of the leaflets of the oil palm tree - Oil Palm Broom Fibres (OPBF), reported impressive physico-mechanical properties. However, information on their bond behaviour with cementitious matrices is presently lacking. This study investigates the bond strength of single and combined OPBF in concrete through direct pull-out tests. Maximum bond strengths of 1.16, 0.95 and 0.82 MPa were recorded at 28, 56 and 112 days respectively. The influence of age of sample and diameter of OPBF tendons on bond strength was observed. Images obtained from scanning electron microscopy reveal embrittlement of fibre surfaces by cement matrix. Finite element modelling of the pull-out behaviour was also carried out using ABAQUS. The potential use of OPBF combined in the form of tendons as longitudinal reinforcement in concrete for lightly loaded structural elements is environmentally friendly and can reduce construction cost.

Keywords: Concrete technology & manufacture; Developing countries; Strength & testing of materials.

List of notations

σ_b	is the bond strength
σ_{28}	is the bond strength at 28 days
σ_{56}	is the bond strength at 56 days
σ_{112}	is the bond strength at 112 days
P	is maximum pull-out load
d_b	is the diameter of tendon/fibre cross-section
L_b	is the embedded fibre/tendon length
σ'	is the nominal traction vector
σ'_i	is the contact traction in a specified direction
σ_i^D	is the contact traction after damage initiation
D	is the scalar damage parameter
d_i	is the direction unique scalar damage variable
K	is the stiffness matrix
δ	is the separation caused by traction
δ_i	is the separation in a specified direction
δ_i^f	is the complete failure separation in a specified direction
$\mathrm{T_e}$	is the element thickness
ε	is elemental strain
F	is the number of fibres per tendon
f'_c	is the compressive strength of concrete
E	is the Young's Modulus
v	is the Poisson ratio

1.0 Introduction

The flexural capacity of plain concrete is generally low and inadequate for most structural application, hence the incorporation of steel in the form of longitudinal reinforcement. Although steel reinforcement possesses good compatibility with concrete and steel-reinforced concrete shows improved mechanical properties such as tensile strength, shear strength, ductility and toughness, it is expensive. Carbon dioxide emissions caused by the production of steel and steel-reinforced concrete are also harmful to the environment. The continuous increase in costs associated with the provision of reinforced concrete infrastructures has also made access to decent housing increasingly difficult in developing countries. In sub-Saharan Africa for example, prevailing factors such as high population growth rates, extreme poverty level among citizens, lack of well-structured housing credit system and inflation have caused serious housing deficits (Bah, *et al.,* 2018). The need for the importation of refined construction materials (e.g. steel), has also resulted in high cost of construction thereby creating the need to search for alternative indigenous building materials.

Unlike steel, which is imported after the process of mining iron ore and subsequent refinement, fibrous plants are readily available in developing countries in the tropics, can easily be replanted and replenished, are considerably more economical to process and are environmentally friendly. The extraction of such fibres is carried out through low energy-intensive procedures such as either cutting the desired plant parts or merely obtaining the plant residues and wastes and subjecting them to retting. The fibres are then usually extracted by manual mechanical separation or by using a decorticator (Onuaguluchi and Banthia, 2016). For instance, a study of energy required for producing conventional reinforcement for concrete showed that 50 times more energy is required for producing conventional steel reinforcement than is required for bamboo reinforcement (Seixa, *et al.,* 2014). Furthermore, plant fibres possess advantages such as low carbon footprint, low-cost, light-weightiness, toughness, thermal insulation, improved acoustic insulation, high recyclability, biodegradability and non-toxicity to the ecosystem (Ramakrishna and Sundararajan, 2005; Ardanuy, *et al.,* 2015; Claramunt, *et al.,* 2016; Agopyan, *et al.,* 2005; Page, *et al.,* 2017). Therefore, the need for researchers and engineers to focus on the possibility of developing low-cost indigenous construction materials from region-specific fibrous plants cannot be overemphasised.

Currently, bamboo stems are the most-studied plant material for longitudinal reinforcement of lightly loaded concrete elements. Ghavami (1995) determined some physical and mechanical properties of bamboo (*Dendrocalamus giganteus*) strips which they were treated with Negrolin and sand and then used to reinforce two 300 x 120 x 3000 mm concrete beams. A comparison between the flexural capacity of the unreinforced concrete beam, the bamboo-reinforced concrete beams and the steel-reinforced concrete beam was carried out. At the recommended bamboo reinforcement ratio of 3%, the bamboo reinforced beam recorded a maximum flexural strength of about 400% and 60% of that of the unreinforced beam and steel-reinforced beam (of 0.78 reinforcement ratio) respectively. Bond strength between the concrete and the bamboo strips were also reported as 0.52 and 0.92 MPa for untreated and treated strips respectively after a bond pull out test. The compressive strength of the concrete was reported as 19 MPa and was obtained by testing 300 x 150 mm cylinders to failure.

Ganesan *et al*. (2018) studied the behaviour of 3 full-scale bamboo-reinforced one-way spanning concrete wall panels. The bamboo strips (obtained from Bambusa bambos) were varnished and sand-blasted prior to their use in M20 concrete. The spacing of the reinforcement strips was carried out according to the requirements of the National Building Code of India-Part 6 (NBC 2016). After 28 days of curing, the wall panels were tested under pinned-end conditions at top and bottom. Loading was applied in a uniformly distributed manner with an eccentricity to simulate real-life scenario. With wall resistance between 700 - 850 kN, the study recommended bamboo reinforced wall panels as viable and sustainable option to steel-reinforced ones. In a similar study by Mali and Datta (2018), the use of bamboo-reinforced concrete slab elements was recommended for use as lightly loaded roofing members for low-cost housing.

Muhtar, *et al*. (2019) improved slip resistance and bond strength of bamboo (*Dendrocalamus asper*) reinforcement in concrete using hose clamps. The samples consisted of an unreinforced concrete beam, an 8 mm steel-reinforced concrete beam and twenty-two 75 x 150 x 1100 mm bamboo-reinforced concrete beams. The bamboo strips were water-proofed by Sikadur® -752 coating after which hose clamps were installed at predetermined distances along the reinforcement strips and a second coating of Sikadur® -752 applied over the whole length. Ultimate failure load in flexure of the bamboo-reinforced concrete (of reinforcement ratio = 4.0%), with hose clamps fixed at 20 mm spacing

around the strips, was greater than the one for control steel-reinforced beam (of reinforcement ratio = 0.89%) by about 26%.

Like bamboo, the ribs of the leaflets of the oil palm tree, otherwise known as oil palm broom fibres (OPBF), have attracted research attention recently due to their impressive mechanical properties (Momoh and Dahunsi, 2017; Momoh and Osofero, 2019; Momoh, *et al.,* 2020). Average tensile strength of OPBF was reported as 389 MPa, density ranged from 450 – 840 kg/m^3 and 24 hours water absorption was reported as 44.7%. The tensile strength to weight ratio of OPBF is about 5 times that of steel, it does not rot easily and has low affinity for water, unlike other vegetable fibres (Momoh, *et al*., 2020). An illustration of different types of fibres from the oil palm tree is presented in the review by Momoh and Osofero (2020). Oil palm fibres such as OPBF can be found in 42 countries spanning the continents of Asia, Africa and South America which totals a land area of about 17 million hectares. Countries with high palm oil production have been reported to face difficulties with managing waste biomass generated from oil palm cultivation and processing activities (Khatun, et al., 2017; Momoh and Osofero, 2020). Current global oil production from oil palm is estimated as 78 million metric tonnes per year with Malaysia and Indonesia being top producers, while Nigeria and Ghana share about 19.5% of global oil palm plantation (Khatun, *et al.*, 2017). Coincidentally, these regions have been continuously plagued with housing deficits. Therefore, the availability of oil palm fibres such as OPBF has attracted research interests for their use in the development of affordable and sustainable building materials in these regions.

A preliminary study on the incorporation of discrete (50mm long) OPBF in concrete was carried out by Momoh and Osofero (2019). The area under the monotonic load-deflection curves of 100 x 100 x 500 mm samples investigated in the study showed improvement in energy absorption by over 300 %. Although no significant improvement in compressive strength was recorded, the improvement in toughness implies a more ductile failure for the OPBF-concrete as against the inherent sudden brittle failure of plain concrete. An enhancement in splitting tensile strength of 1.2% at 28 days was also reported in the same study (Momoh and Osofero, 2019).

OPBF like other vegetable fibres are naturally functionally graded and anisotropic with mechanical properties varying in both the longitudinal and radial directions. However, structural reinforcements can be developed from the vegetable fibres if combined in the form of tendons (Momoh and Dahunsi,

2017). Figure 1.1 illustrates the locations of OPBF on an oil palm leaf and some extracted OPBF tied into broom units. The OPBF are the ribs of the leaflets of the oil palm tree usually extracted by scraping off the leaflets from the ribs with the aid of a hand knife. The fibres are then tied as broom units (Figure 1.1 c) with each unit consisting of between 500-1000 fibres to be sold in local markets for approximately 0.1 USD per unit and even for a lesser amount in rural areas.

The major factors responsible for the improvement of mechanical properties of fibre-reinforced composites are the mechanical properties of the reinforcing fibres, shape and geometry of the fibres, fibre dosage, fibre orientation and fibre-matrix adhesion. Mechanical properties of some vegetable fibres used for reinforcing cementitious composites are presented in Table 1.1. Due to the relatively high tensile strength of vegetable fibres, the failure mode of most natural fibre-reinforced cementitious composites is characterised by fibre pull-out from the matrix. A well-established method for the characterisation of fibre/matrix interface is the single fibre pull-out experiment (Naik, *et al.,* 2019; Soulioti, *et al.,* 2013) where an axial force is applied unto the tip of a fibre in order to pull it out of a host matrix.

Studies on the bond behaviour of concrete-steel fibres (Soulioti, *et al.,* 2013), concrete-Fibre Reinforced Polymer bars (Zenon and Pilakoutas, 2004), polypropylene-cement matrix (Singh, *et al.,* 2004) and natural fibre-cement matrix (Naik, *et al.,* 2019; Ramakrishna and Priyadharshini, 2018; Ferreira, *et al.,* 2018) show that transfer of forces from fibres or reinforcement bars onto matrix is dependent on three mechanisms: chemical adhesion, mechanical anchorage and frictional force (Ramakrishna and Priyadharshini, 2018; Ferreira, *et al.,* 2016). Other influential parameters include concrete cover, bar embedded length, bar size and yield strength (ACI 408R-03, 2003; Issa and Masri, 2015). Axial force applied to a reinforcement bar creates both tangential and parallel stress components along the bar-concrete contact surface. The parallel stress component is known as bond stress (Hadi, 2008). Bond force, therefore, is the force required to move a bar parallel to its length with respect to the surrounding matrix. Knowledge of bond stress, usually obtained from pull-out tests, is required for understanding the transition zone, the resistance to crack propagation and also for predicting composite mechanical performance (Savastano and Agopyan, 1999). Although the pull-out test procedure results in higher values of bond strength than is possible to achieve in practice, for

example where maximum bond depends on cover thickness, it offers an economic and simple procedure (Zenon and Pilakoutas, 2004; Osofero, *et al.,* 2015).

While most of the natural fibres presented in Table 1.1 are superior to steel in terms of tensile strength-to-weight ratio, their range of Young's modulus which is about 1.4 – 22 % of the Young's modulus of steel may pose serviceability concerns in structural design. This entails devising a different design approach with special recommendations. Consequently, the need to adequately understand their bond behaviour with cementitious matrices becomes a fundamental preliminary task.

Table 1.1. Mechanical properties of some vegetable fibres used in cement composites

Vegetable Fibre	**Average tensile strength (MPa)**	**Average Young's modulus (GPa)**	**Density (kg/m^3)**	**Reference**
OPBF	389.5	9	450-840	Momoh *et al.* (2020)
Jute	250	44	-	Ferreira *et al*. (2016)
Sisal	400	19	-	Silva *et al*. (2011)
Date Palm Fibre	93.4	2.7	720	Hamid and Abdelmadjid (2016)
Coconut	95-118	2.8	1177	Pacheco-Torgal and Jalali (2011)
Wheat straw	47	3.9	-	Naik *et al.* (2019)
Piassava	143	5.6	1054	Pacheco-Torgal and Jalali (2010
Bamboo (*D. asper*)	126.7	17	-	Muhtar *et al*. (2019)
Bamboo (*B. arundinacea)*	200	8	1125	Malli and Datta (2018)
Bamboo (*B. vulgaris*)	141	13	720	Ghavami (1995)
Polypropylene	250	2	913	Pacheco-Torgal Jalali (2010)
CFRP	>15	115	-	Zenon and Pilakoutas (2004)
GFRP	>1000	45	-	Zenon and Pilakoutas (2004)
Steel	400*	207.7	8700	Muhtar *et al.* (2019)

CFRP = carbon fibre-reinforced polymer; GFRP = glass fibre-reinforced polymer *yield strength

1.1 Bond behaviour of natural fibres in cementitious matrix

Bond pull-out curves for most natural fibres in cement composites are characterised by three main stages, namely: perfectly-bonded stage, partially-debonded stage and fully-debonded stage (Wan and Parris, 2016). Figure 1.2 illustrates a typical pull-out response of a single OPBF from a concrete

matrix (Momoh and Osofero, 2019). The response at the perfectly bonded stage is almost linear. Debonding begins at the region where the fibre meets the matrix and travels through the matrix along the fibre-matrix interface, marking the onset of a non-linear response. As the pull-out force on the fibre becomes greater than the bond stress, the slope of the curve flattens out or sometimes drops abruptly at complete debonding. Pull-out response for natural fibres after complete debonding from their matrix can be classified as either: slip-hardening, constant friction or slip-softening (Naik, *et al.,* 2019). At complete debonding, chemical adhesion expires, and the response becomes predominantly due to mechanical interlocking and friction. Major factors affecting post-debonded stage response are purity of fibre surface, roughness of fibre surface, shape of fibre, embedded fibre length and fibre/matrix strength ratio.

For vegetable fibres in cementitious matrix, the degradation of fibre surface due to alkali attack causes slip softening, as the fibre-matrix interface becomes separated by an organic layer (Wan and Parris, 2016; Wei and Meyer, 2015). Such layer creates a lubricating effect thereby facilitating slip. Consequently, chemical treatments for enhancing the resistance of natural fibres to surface deterioration by alkali have been successful in previous research (Wei and Meyer, 2014). The area under the bond stress *versus* slip curve is the energy required for complete pull out of the fibre from the matrix. It follows from Figure 1.2 that the area under the curve from the onset of loading to the end of the partially bonded stage is the energy dissipated in debonding the fibre from the matrix. In other words, it is referred to as *debonding energy* while the area under the fully-debonded stage is the *pull-out energy* (Naik, *et al.,* 2019).

Due to high variability in physico-mechanical properties of natural fibres and different experimental procedures, different values of embedded lengths are recommended. For example, different optimum embedded length for sisal fibres was determined by previous studies as 30 mm (Morrissey, *et al.,* 1985) and 40 mm (Silva, *et al.,* 2011). Morrissey, *et al*. (1985) prepared and tested a total of 210 samples of sisal fibres embedded in ordinary Portland cement matrix of water-cement ratio of 0.4 (by weight). The mean cross-sectional radius of the fibres was recorded as 0.21 mm ± 0.04 mm and they were embedded in the matrix at 10, 15, 20, 30, 40, 50 and 60 mm and pulled out of the matrix at a displacement control rate of 10 mm/minute. Silva, *et al.* (2011) on the other hand, embedded 6 samples of sisal fibres with similar cross-sections in a mortar matrix mix of 1:1:0.4 binder/sand/water

248 (by weight) respectively. The specific weight of the river sand used was 2.67. The binder consisted of
249 Portland cement CPII F-32 and 5% (by volume) of wollastonite as micro reinforcement and a
250 naphthalene plasticiser to enhance the tensile strength and rheology of the matrix. The fibres were
251 embedded at lengths ranging from 10 – 40 mm and pulled out at a speed of 0.1 mm/min. The loading
252 rate applied in testing the samples makes comparison of results obtained from the study with that
253 from the study of Morrissey, *et al*. (1985) difficult. Other recommendations of optimum embedded
254 length obtained from pull out test of natural fibres in cement/sand mortar include, 40 mm for date palm
255 fibres with a cross-sectional diameter of 0.55 mm and embedded in cement-sand matrix (Hamid and
256 Abdelmadjid, 2016), 20 mm for wheat straw with cross-sectional diameter of 1.14 mm and embedded
257 in cement-clay matrix (Naik, *et al.,* 2019) and 25 mm for sisal and coir with cross-sectional diameters
258 of 0.13 mm and 0.40 mm respectively, embedded in cement-sand matrix (Ramakrishna and
259 Priyadharshini, 2018). Experimental assessment of bond behaviour of jute fibres having embedded
260 lengths of 5mm and 10 mm in (1:0.5:0.4) cement/sand/water mortar reported a bond strength ranging
261 between 0.17-0.46 MPa with fibre pull-out as the major failure mode (Ferreira, *et al.,* 2016). This is
262 similar to 0.36-0.38 MPa range reported for sisal fibres in (1:1:0.4) cement/sand/water matrix (Silva, *et*
263 *al.,* 2011), 0.23-0.3 MPa for wheat straw in (1:1:1) cement/clay/water (Naik, *et al.,* 2019) and 0.05-
264 0.33 MPa for date palm fibres in (1:3:0.55) cement/sand/water matrix (Hamid and Abdelmadjid, 2016).
265 In addition, bond strength variability with age (for up to 28 days) was observed in (Ramakrishna and
266 Priyadharshini, 2018) to increase for sisal fibres, but decreased for coir.

267 Bond pull-out behaviour for plant parts of larger dimensions, like bamboo culms, in concrete is similar
268 to that of smaller fibres. Varying bond strength values for bamboo in concrete were also reported;
269 e.g., 0.41 MPa for an embedded length of 300 mm in 12 MPa concrete (Nindyawati and Umniati,
270 2016) and 1.74 MPa at an embedded length of 150 mm in 30 MPa (cube strength) concrete (Sakaray,
271 *et al.,* 2012). In another study, a bond strength value of between 0.14 – 1.4 MPa was reported for
272 surface-treated bamboo at an embedded length of 100 mm in 20 MPa (cube strength) concrete (Mali
273 and Datta, 2019). Ghavami (1995) reported 0.52 MPa for an embedded length of 100 mm in 19 MPa
274 (cylinder strength) concrete, while Kute and Wakchaure (2013) reported bond strength values of 0.73
275 - 0.9 MPa for untreated bamboo at an embedded length of 150 mm in 20 MPa (cube strength)
276 concrete. These indicate that bond strength increases with an increase in both the compressive
277 strength of concrete and embedded length of the fibre. Similar to smaller vegetable fibres behaviour,

the predominant failure mode is debonding and pull-out of the bamboo fibres. It is important to note, however, that the bond behaviour of single small fibres in a cementitious matrix may be different from that of combined fibres or typical single reinforcement bars.

Although OPBF are reported as being superior to steel reinforcement in terms of tensile strength-to-weight ratio and may be combined in the form of tendons for the purpose of reinforcing concrete (Momoh *et al*., 2020), research interest in OPBF is recent and a study on their bond behaviour with concrete is non-existent at the moment. Therefore, bond behaviour of single OPBF and combined OPBF (in form of tendons) was investigated. In addition, the effect of age of the composite on bond strength was observed. Finally, a 3D-nonlinear finite element model capable of simulating the experimental bond-slip relationship between OPBF and concrete was carried out. This study will enhance decision-making in the design and use of the natural fibres for reinforcing load-bearing cementitious elements.

2. Materials and Method

2.1 Experimental study

Cement, coarse and fine aggregates were obtained from *Jewson Ltd, Aberdeen, UK,* while OPBF were obtained from *Rice and Spice, Aberdeen, UK*, in the form of broom units. The OPBF were not subjected to any form of pre-treatment. From trial mixes, an average 28-days compressive strength of 30 MPa (cylinder strength) was achieved for a mix ratio of 1:1.5:3 cement, fine aggregate and coarse aggregate, respectively (by volume), at a water-cement ratio of 0.52 and a slump value of 95 mm. This grade of concrete is adequate for construction of residential buildings (Singh and Scanlon, 2013). Particle size grading of aggregates was carried out according to ASTM C136/C136M (2014). The fine aggregate used was river sand while the coarse aggregate was naturally weathered igneous rock (pea gravel). Constituents of concrete used, and particle size distribution curves are presented in Figure 2.1. Specific gravities of fine aggregate classified as *medium sand* and coarse aggregate classified as *fine gravel* were 2.55 and 2.62, respectively. General-purpose cement (Blue circle®) was used as the binder. Concrete mixing procedure commenced with the pouring of the required amount of water in a 25-litres electrically-powered mixing drum, followed by the addition of respective quantities of aggregates.

306 Samples were prepared for both single fibre pull-out and combined fibre pull-out testing in order to
307 understand possible differences between the bond behaviour of single OPBF and combined OPBF
308 tendons. For the latter, OPBF were combined in the form of twisted tendons where individual fibres
309 were wound around themselves (in a helical shape) in the same direction and held in position radially
310 by aluminium wires of 1mm diameter (see Figure 2.2). Like other plant fibres, the flexibility of OPBF is
311 dependent on the moisture content. Moisture content of the OPBF was determined according to the
312 requirements of ASTM D4442 (2016) as 9.81% and density as 840 kg/m^3. Details of physical and
313 mechanical properties of OPBF are presented in a previous study by the authors (Momoh *et al.* 2020).
314 Winding of OPBF around themselves to form tendons was carried out to the extent to which the
315 flexibility of individual fibres could allow without breakage. Approximate distances along the length of
316 respective tendons for each complete cycle of winding were measured as 30 mm, 50 mm, 70 mm,
317 100 mm and 140 mm for 2, 3, 4, 5 and 6 fibres respectively. The OPBF tendons were then cut into
318 lengths of 200 mm, after which one end of each tendon was dipped in epoxy glue to form a thick bulb
319 of glue around it. This was done to prevent the tendons from being damaged by the grips of the
320 universal testing machine. A thin layer of epoxy was then applied around the tendons from the glue
321 bulb, down to 80 mm before tendon-end such that 80mm of each tendon was embedded in the
322 concrete matrix. This was done to prevent moisture-induced premature weakening of fibres having
323 direct contact with moisture during curing. Weakening of the tendons would result in tensile failure of
324 tendon itself instead of bond failure with concrete during pull-out test. The cross-section of the
325 opposite end of the tendons were smeared with epoxy glue and the aluminium wires were removed
326 after the glue had set. Figure 2.3 presents a schematic diagram of the test set up.

327 Cubic moulds of 100 mm were placed on a vibrating table and filled with concrete. The OPBF tendons
328 were inserted in the fresh concrete to an embedded length of 80mm and held in position by hand as
329 the concrete was vibrated. At the end of the vibration, the sample was left to air-cure at room
330 temperature for 24 hours after which they were demoulded and immersed in a curing tank with water
331 level just at the top level of the concrete (Figure 2.4). Submerging of whole sample was avoided to
332 prevent excessive soaking (and possible weakening) of OPBF tendon. At the specified test dates, the
333 samples were removed from the water, left to stand for about 2 hours and wiped dry with a soft paper
334 towel. Testing was carried out on a Hounsfield universal testing machine (Model H10KS) with a 3kN

load cell in displacement control at 2.5mm/min. Uniform bond between OPBF and concrete was assumed, and bond strength was calculated according to Eqn 2.1.

$$\sigma_b = \frac{P}{\pi d_b L_b}, \ldots\ldots\ldots\ldots\ldots\ldots\ldots\ldots\ldots\ldots\ldots\ldots\ldots\ldots\ldots\ldots\ldots\ldots\ldots\ldots\ldots\ldots\ldots\ldots\ldots\ldots\ldots\ldots\ldots\ldots\ldots\ldots\ldots\ldots\ldots\ldots. \quad 2.1$$

where σ_b is the *bond strength*, *P* is *maximum pull-out load*, d_b, is the *diameter of tendon cross-section* and L_b is the *embedded fibre/tendon length*. The cross-sectional area of each OPBF-tendon was assumed to be circular and was measured using a digital veneer calliper with a precision of 0.01mm.

A total of fifty-four (54) specimens were prepared, cured and tested. Testing was carried out at 28, 56 and 112 days of curing. Sample designation is explained as: XF-YYY such that X stands for the number of fibres in the tendon, F stands for fibres and YYY stands for the age of sample at testing (in days). For example, 6F-028 refers to an OPBF tendon consisting of 6 fibres and tested at 28 days in direct bond-pull out. Similarly, 2F-112 is an OPBF tendon consisting of 2 fibres and tested at 112 days. Sample preparation and testing were carried out in the cement and materials laboratory of the School of Engineering, University of Aberdeen, UK.

Scanning Electron Microscopy (SEM) images of OPBF surface before insertion in the concrete matrix and after pull-out were obtained using a *CarlZeiss GeminiSEM 300VP* scanning electron microscope. About 20nm-thick carbon coating was applied over the OPBF surfaces and followed by approximately 10nm-thick sputter coating of gold/palladium alloy (60% Au and 40% Pd) in order to enhance the conductivity of the samples. SEM was performed using the facilities at the Aberdeen Centre for Electron Microscopy, Analysis and Characterisation (ACEMAC), University of Aberdeen, UK.

2.2 Modelling of bond behaviour

Modelling of reinforced concrete behaviour can be achieved through three different approaches: distributed, embedded and discrete, with the first two approaches assuming perfect bonding between matrix and reinforcement (Issa and Masri, 2015; Khalfallah and Ouchenane, 2007). Perfect bonding is, however, difficult to realise in practice, hence the use of discrete approach for modelling of composites (Jendele and Cervenka, 2006).

An efficient finite element methodology to represent interfacial deterioration is surface-based cohesive contact modelling (Alizadeh, 2019; Farzad, *et al.,* 2014; Omar, *et al.,* 2014). Surface-based cohesive

models are suitable for problems where interfacial strength is relatively weak compared to the material properties of the bodies in contact (Camanho and Dávila, 2002) and where the interfacial thickness is negligible (Farzad, *et al.,* 2014). Cohesive contact modelling can also simulate the progression of damage without the need to define an initial crack, unlike in classical fracture mechanics modelling (Campilho, *et al.,* 2011; Ali, *et al.,* 2019). The surfaces in contact can also stick after separation (Bendetti and Aliabadi, 2013). Modelling of contact between the surfaces uses the traction-separation constitutive relationship and contact is defined as a surface interaction property rather than a material property (Farzad, *et al.,* 2014). The cohesive surface model has reduced mesh-sensitivity and does not require the mass of the materials since it is defined as an interface property, thereby reducing computational efforts (Ramamurthi, *et al.,* 2013). Although the cohesive models in ABAQUS were originally developed for the simulation of delamination in composites (Ali, *et al.,* 2019; Pereira, *et al.,* 2015), their appropriateness for simulation of pull-out behaviour has been demonstrated in (Khalfallah and Ouchenane, 2007; Serpieri, *et al.,* 2015; Fantilli and Vallini, 2007).

Surface-based cohesive contact method was employed in this study to simulate the bond behaviour between OPBF and concrete. A general elastic constitutive matrix that relates nominal stresses to nominal strains of an element of finite thickness across the interface can be defined as Eqn 2.2 (Farzad, *et al.,* 2014):

$$\sigma' = \begin{Bmatrix} \sigma'_n \\ \sigma'_s \\ \sigma'_t \end{Bmatrix} = \begin{bmatrix} K_{nn} & K_{ns} & K_{nt} \\ K_{ns} & K_{ss} & K_{st} \\ K_{nt} & K_{st} & K_{tt} \end{bmatrix} \begin{Bmatrix} \delta_n \\ \delta_s \\ \delta_t \end{Bmatrix} = K\delta, \quad \text{2.2}$$

where σ' is the *nominal traction vector*, *K* is the *stiffness matrix* and δ is the corresponding separation each having components in the normal direction (subscript *n*) and the two shear directions (subscripts *s* and *t*). The nominal stresses and strains are the force components divided by original area and separations divided by original thickness, respectively, at each integration point. For a 3-dimensional cohesive element with thickness T_e and strains ε, the separations can be expressed as:

$$\delta_n = \varepsilon_n T_e\,, \qquad \delta_s = \varepsilon_s T_e\,, \qquad \delta_t = \varepsilon_t T_e\,.$$

In ABAQUS, constitutive thickness of the cohesive surface is assumed to have a unit value (Ramamurthi, *et al.,* 2013). For pure normal separation where cohesive forces in the shear directions are zero, and pure shear slip yields zero normal separation, Eqn 2.2 can be simplified and only

K_{nn}, K_{ss} and K_{tt} are defined. For an isotropic material, the stiffness K is used everywhere because the values in all directions are the same (Ramamurthi, *et al.,* 2013).

Relative motion between the interacting surfaces can be chosen as “finite sliding”, “infinitesimal sliding” or “small sliding”. Small sliding interacting surface model was used in this study as it allows for relatively little sliding of one surface along the other, based on linearised approximations of the master surface per constraint. In addition, it is computationally less expensive than finite sliding, particularly for 3-dimensional contact modelling (ABAQUS, 2019). This means that an initial linear elastic bond behaviour (interface stiffness) ends at the maximum bond stress (damage initiation criterion) and is followed by degradation of interface stiffness (damage evolution criterion) (Sun and Jin, 2012). Damage initiation refers to the beginning of degradation of the cohesive response at a contact point by setting limits for the contact stresses and/or contact separations. Beyond the set limit, the process of degradation of interface bond commences.

The linear post-damage initiation softening response is defined for the degradation of interface stiffness using damage evolution criterion. Figure 2.5 shows a representation of a traction-separation response. The damage evolution law specifies a scalar damage parameter *D* which evolves from *0* to *1* upon further loading after damage is initiated (Campilhoa, *et al.,* 2008) such that:

$$\sigma_i^D = (1 - D)\sigma'_i \quad \ldots\ldots 2.3$$

Where, σ_i^D is the contact stress after damage initiation and σ'_i is the contact traction at normal and shear directions (*i*). For complete failure separation δ_i^f and maximum relative displacement δ_i^{max} , the irreversible, bilinear, softening behaviour represented in Figure 2.5 was developed by Camanho and Dávila (2002) and defined by Eqn 2.4.

$$\sigma'_i = \begin{cases} K\delta_i & \leftarrow \delta_i^{max} \le \delta_i^o \\ (1 - d_i)K\delta_i & \leftarrow \delta_i^o < \delta_i^{max} < \delta_i^f \\ 0 & \leftarrow \delta_i^{max} \ge \delta_i^f \end{cases} \quad \ldots\ldots 2.4$$

where d_i is the direction unique scalar damage variable defined by Eqn 2.5

$$d_i = \frac{\delta_i^f(\delta_i^{max} - \delta_i^o)}{\delta_i^{max}\left(\delta_i^f - \delta_i^o\right)} \qquad d_i \in [0,1] \quad \ldots\ldots 2.5$$

For the model described beyond δ_i^f the interface becomes traction-free (i.e. are under no stress).

The maximum stress criterion (Eqn 2.6) and the maximum separation criterion (Eqn 2.7) are the two damage initiation criteria applied for the interface:

$$max\left\{\frac{\langle\sigma_n\rangle}{\sigma_n^o},\frac{\sigma_s}{\sigma_s^o},\frac{\sigma_t}{\sigma_t^o}\right\}=1, \ldots\ldots\ldots\ldots\ldots\ldots \quad 2.6$$

$$max\left\{\frac{\langle\delta_n\rangle}{\delta_n^o},\frac{\delta_s}{\delta_s^o},\frac{\delta_t}{\delta_t^o}\right\}=1, \ldots\ldots\ldots\ldots\ldots\ldots \quad 2.7$$

where σ_n^o, σ_s^o and σ_t^o are the peak values of the contact stress when the separation is either purely normal to the interface or purely in the first and second shear direction, respectively. The same definition applies to the peak values of contact separation $\delta_n^o, \delta_s^o, \delta_t^o$. Macaulay brackets $\langle\quad\rangle$ are used for the contact stress normal to the interface to emphasise that damage is not initiated by a purely compressive stress state (Omar, *et al.,* 2014; Ramamurthi, *et al.,* 2013; Campilho, *et al.,* 2011).

2.2.1 Finite Element modelling of OPBF-concrete bond

Perfect bonding does not exist between OPBF and concrete, hence, the discrete approach of finite element modelling was employed. Three-dimensional modelling was used to simulate the pull-out behaviour of OPBF in concrete matrix. Interfacial deterioration during pull-out was modelled using surface-based cohesive contact modelling. The ability of model surfaces to stick is representative of bond behaviour between OPBF and concrete which does not deteriorate completely for the experimental pull-out distance. Concrete and OPBF were modelled using 8-node linear brick elements with reduced integration (C3D8R). Both concrete and OPBF dimensions were consistent with the physical pull-out samples with a circular cross-section assumed for the tendons: i.e., 100 x 100 x 100 mm for the concrete matrix and cross-sectional diameters of 1.20 mm, 2.10 mm, 3.00 mm, 3.10 mm, 3.70 mm and 3.82 mm for 1F, 2F, 3F, 4F, 5F and 6F tendons respectively. Each tendon was 200 mm in length.

The 100 mm cubic homogeneous solid was assigned the material properties of the concrete as obtained from the experiments. Each cube model had a circular opening with a diameter corresponding to the respective OPBF-tendon and running through from the top centre-face to the bottom centre-face of the concrete model cube. OPBF-tendons were also modelled as homogeneous solids and assigned corresponding average elastic properties obtained from the experiments. Each OPBF-tendon was inserted into the opening of the concrete cube such that a cohesive surface length

(embedded length from experiment) of 80 mm was achieved. See Table 2.1 for material properties used in the numerical models.

Concrete was taken as the master surface while OPBF tendon was taken as the slave surface. Two boundary conditions were defined for the models: firstly, an “encastre” to rigidly fix the top of the concrete cube and a “displacement” of 8 mm applied to the free end of the OPBF tendon in the pull-out direction. This generated the force required to pull out the tendon from the concrete for the applied displacement. The displacement was applied in small increments of 0.1 mm to avoid numerical instability. Mesh sizes used were 5 mm and 10 mm in the length direction for the concrete and OPBF respectively. However, finer mesh size was used around the interaction region between the two materials in order to enhance the accuracy of the results. Coarser meshes were used for concrete region farther away from the OPBF in order to reduce computational time. From the experiments, over 60% loss in the bond stress was recorded at 20 mm slip of OPBF-tendons, hence a final separation distance δ_i^f of 20 mm was specified for the models. The problem was solved using ABAQUS’ standard static procedure. Figure 2.6 presents visualisation of the finite element modelling of OPBF pull-out from concrete.

Table 2.1: Material properties used in bond pull out models

Material	**Compressive strength** f_c' (MPa)	**Tensile strength** fy (MPa)	**Youngs Modulus** *E* (GPa)	**Poisson’s ratio** *v*
Concrete	30	--	25	0.15
OPBF-tendon	--	389	9	0.4

3. Discussion of Results

Table 3.1 and Figure 3.1 shows results (with standard deviations) of pull-out test of OPBF from concrete. Sample failure was governed by tendon pull-out from concrete matrix. Average pull-out curves of the samples are shown in Figures 3.1 (a,b,c) at 28, 56 and 112 days, respectively. Generally, bond strength between concrete and OPBF reduced with age and increased with an increase in the number of individual OPBF per tendon. Average percentage loss in bond strength at 112 days for single OPBF was 41% while that for OPBF tendons was 25%. Reductions in bond

strength was due to interface degradation caused by the action of cement alkali on the surface of the OPBF (Momoh and Osofero, 2019; Karade, 2010). Fibre surface degradation was however reduced for the tendons because the combination of multiple fibres prevented contact between the entire surface of each individual OPBF and the cementitious matrix.

Table 3.1: Results from pull-out experiment of OPBF from concrete

Sample ID.	**Surface area of OPBF Tendon (mm^2)**	**Embedded length (mm)**	**Average Peak Load P (N)**	**Bond strength σ_b (MPa) standard deviation in bracket**	**Percentage reduction in bond strength at 56 and 112 days (%)**	**Failure Mode**
1F-028	235.61	80	131.33	0.56 (0.167)	-	pull-out
2F-028	530.00	80	306.6	0.58 (0.042)	-	pull-out
3F-028	754.00	80	551.65	0.73 (0.008)	-	pull-out
4F-028	770.00	80	654.80	0.85 (0.1185)	-	pull-out
5F-028	900.00	80	822.00	0.91 (0.002)	-	pull-out
6F-028	939.30	80	1092.00	1.16 (0.193)	-	pull-out
1F-056	235.61	80	77.4	0.33 (0.026)	41.07	pull-out
2F-056	530.00	80	217.10	0.41 (0.089)	29.31	pull-out
3F-056	754.00	80	333.20	0.44 (0.084)	39.72	pull-out
4F-056	770.00	80	540.40	0.70 (0.026)	17.65	pull-out
5F-056	900.00	80	855.00	0.95 (0.134)	-4.40	pull-out
6F-056	939.30	80	843.00	0.90 (0.026)	22.41	grip
1F-112	235.61	80	77.75	0.33 (0.052)	41.07	pull-out
2F-112	530.00	80	217.04	0.41 (0.134)	29.31	pull-out
3F-112	754.00	80	369.46	0.49 (0.035)	32.88	pull-out
4F-112	770.00	80	477.40	0.62 (0.129)	27.06	pull-out
5F-112	900.00	80	729.00	0.81 (0.263)	10.99	grip
6F-112	939.30	80	770.23	0.82 (0.208)	29.31	pull-out

The surface undulation of the tendons created by the helical winding of individual OPBF also resulted in mechanical anchorage for increased bond resistance.

Observation of the mechanism of debonding of OPBF from the concrete matrix revealed that tendon pull-out and tear were observed beyond 56 days. While single fibre pull-out was characterised by gradual debonding and subsequent pulling out of fibres, OPBF tendon pull-out was characterised by debonding, followed by mechanical interlocking, then a combination of damage of individual fibres and mechanical interlocking, and finally fracture/tearing of individual OPBF making up the tendon. This is reflected as a predominant slip-softening behaviour for single OPBF as the bond stress decayed rapidly after the maximum value. On the other hand, slip-hardening was observed for most OPBF tendons such that a residual bond strength was maintained beyond the maximum value (see Figure 3.1). Damage to tendons was proportional to the number of individual OPBF making up the tendon. Figure 3.2 illustrates the damage to OPBF tendons after a forceful complete pull-out from the concrete matrix at 112 days. This mechanism of failure leads to increase in energy absorption of OPBF-concrete composite, a phenomenon observed in a previous study (Momoh and Osofero, 2019) for random inclusion of OPBF in the form of 50 mm discrete fibres in concrete. Pull-out of OPBF tendons without corresponding damage to concrete also imply that the shear stress borne by concrete matrix was low.

SEM images revealing the embrittlement of OPBF surface, at 112 days, by cement alkali of the concrete matrix are presented in Figure 3.3. Alkali embrittlement, with time, resulted in the formation of an organic layer between the OPBF and the matrix, thus causing reduced shear resistance at the interface of the two materials. Consequently, adhesion between OPBF and the surrounding matrix deteriorated and resulted in reductions in bond strength with age of samples reported in Table 3.1 as percentage reduction in bond strength. Notwithstanding, an increase in the number of individual OPBF per tendon resulted in increased mechanical interlock with the concrete matrix. Consequently, linear correlations were observed between tendon size and bond stress at 28, 56 and 112 days (see Figure 3.4).

The maximum values of bond strength obtained in the study of Ramakrishna and Priyadharshini (2018) for coir in 1:3 cement-sand mortar are about 40% of OPBF-concrete bond strength at 28 days. At 112 days, reduction in bond strength of OPBF was recorded. However, these values (0.33-0.82

MPa) are still higher than the range reported for other types of fibres in literature: (0.17-0.46 MPa) for jute fibres in cement mortar at 7 days (Ferreira, *et al.,* 2016), (0.36-0.38 MPa) for sisal fibre in cement mortar at 28 days (Silva, *et al.,* 2011) and (0.4-0.5 MPa) for polypropylene fibres in cement mortar at 28 days (Singh, *et al.,* 2004). Maximum bond strength obtained at 28 days from this study (with 80 mm embedded length) is 66% of bond strength reported in (Sakaray, *et al.,* 2012) for bamboo strips (at an embedded length of 150 mm) in grade-30 concrete. It should be noted that using a similar embedded length of OPBF tendons (i.e. beyond 80 mm) would cause an increase in mechanical interlock due to the helical arrangement of the fibres constituting the tendon, and hence result in higher values of bond strength. In addition, bond strength of OPBF reported in this study is about 14% of the reported bond strength between concrete and reinforcing steel bars (at an embedded length of 150 mm) in grade-30 concrete at 28 days (Sakaray, *et al.,* 2012). With an increased embedded length of OPBF tendons, bond strength would be adequate for lightly loaded elements like lintel beams of low-cost farm houses. Furthermore, the comparison of bond strength of OPBF with the range for untreated bamboo (0.73-0.9 MPa) at an embedded length of 150mm in grade-20 concrete (Kute and Wakchaure, 2013) and surface treated bamboo (0.14-1.4 MPa) at an embedded length of 100 mm in grade-20 concrete (Mali and Datta, 2019), show that surface-treated OPBF with similar embedded length and grade of concrete could produce superior bond results. On the other hand, it is also important to note that the reported studies investigated different species of bamboo with varying mechanical properties, hence, an in-depth study on bond behaviour of OPBF from different oil palm trees and in various grades of concrete as well as at varying embedded lengths is also necessary.

Lack of bond-strength results beyond 28 days makes the comparison between values obtained from literature, with that for OPBF in concrete, difficult. However, a comparison between the 112 days bond strength of single OPBF and tendons with the 28 days bond strengths reported for other vegetable fibres, indicate that the surface of OPBF has good resistance to surface degradation. This preserved the bond strength with time and implies a superior performance for OPBF as reinforcement for cementitious matrices. Oil palm fibres have good resistance to deterioration due to the high content of silica bodies on the surface (Omar, *et al.,* 2014).

The resulting finite element simulation (Figure 2.5) also shows that stress in the concrete is minimum thereby corroborating the pull-out of OPBF tendons without damage to surrounding concrete as

observed in the experiment. Therefore, the cohesive surface bond model is adequate for simulating bond between concrete and the OPBF-tendons. Figure 3.5 shows the accuracy of the numerical model as validated with the experimental results at 28 days. Numerical modelling of time rate of degradation of concrete/OPBF interface should be investigated in order to accurately predict bond strength in the long term. The use of finite element simulation would enable parametric studies that would otherwise be difficult and time-consuming with physical experiments.

From the correlation between bond strength and number of OPBF per tendon shown in Figure 3.4, linear relationships were derived and are shown in Eqns 3.1-3.3.

$\sigma_{28} = 0.1174F + 0.3873$, ($R^2 = 0.946$)……..…….3.1

$\sigma_{56} = 0.1351F + 0.1487$, ($R^2 = 0.902$)……..……3.2

$\sigma_{112} = 0.108F + 0.2020$, ($R^2 = 0.965$)……..…….……...3.3

where σ_{28}, σ_{56} and σ_{112} are the bond strengths at 28, 56 and 112 days, respectively, and ($1 \leq F \leq 6$) is the number of OPBF in the tendon. The R^2 values of 0.946, 0.902 and 0.965 of Eqns 3.1-3.3 for bond strengths 28, 56 and 112 days, respectively, show a strong correlation between bond stress and number of individual OPBF making up a tendon.

An obvious superiority of conventional steel reinforcement over plant fibres is the high shear resistance of the surface of the reinforcement. While steel is homogeneous and is not embrittled by cement alkali, plant fibres surfaces undergo alkali-induced degradation, thereby weakening and resulting in loss adhesion with surrounding concrete. Consequently, bond strength reduces with time as the degrading action at the matrix-fibre interface progresses. It is reported that time-related degradation of vegetable fibres surface, in cement alkali, can be minimised by pre-treating fibres with alkali solution (Machaka, et al., 2014) or silane solution (Blankenhorn, et al., 2001). Although these treatments are currently being investigated for their effectiveness in enhancing bond behaviour of OPBF tendons in concrete matrix, they have been proven for discrete plant fibres meant for random distribution in cementitious matrices. For practicality, factors such as cost of treatment, recovery of chemicals from effluents or environmental impact of effluent disposal should be measured against the target improvement desired for the composite. Possible ways of improving shear resistance of the surface of natural reinforcements include pre-coating the reinforcement surfaces with structural adhesives (Agarwal *et al*., 2014) and the use of shear connectors (in form of hose clamps) to

maximise mechanical interlocking and shear transfer between the reinforcement and host matrix (Muhtar *et al*., 2019). A combination of both enhancement strategies could result in a hybrid reinforcement material and is an area for further research. Combining OPBF into tendons using hose clamps would mobilise the full tension capacity of the tendons in the matrix. Hence subsequent studies by the authors on the use of OPBF as structural reinforcement analogous to bamboo reinforcement would consider the use of hose clamps as shear connectors.

A comparison of bond strength between concrete and structural materials such as steel and bamboo is presented in Table 3.2. Bond strength between OPBF and concrete at 28 days is about 40% of that of thermo-mechanically treated (TMT) steel and 65% of that of mild steel. At 112 days, it reduces to about 29% of TMT steel and 46% of that of mild steel. Though bamboo is the most-recommended natural reinforcement for concrete, it is difficult to compare its long-term bond performance with OPBF's as most studies are limited to 28 days values. However, the 112 days bond strength value for OPBF tendons competes favourably with the 28 days bond strength of untreated bamboo in similar matrix. Long-term performance of OPBF in concrete is currently a grey area of research. Therefore, further investigation is required in this direction. For practical application of OPBF tendons for reinforcement in concrete, a study of the time-rate of interface degradation needs to be carried out to assess long term performance of the composite. Furthermore, the correlation between tendon size (of above 6 OPBF per tendon) and bond strength requires further study. Although it is obvious that the combination of multiple fibres in form of tendons prevents contact between the entire surfaces of individual OPBF and the cementitious matrix, the limit at which this linear relationship (Figure 3.4) ceases to exist will inform OPBF- reinforced concrete design procedure and recommendations.

587 Table 3.2: Comparison of bond strength of Steel, OPBF and Bamboo in concrete

Material	28 days bond strength (MPa)	Embedded length (mm)	Compressive strength of concrete (MPa)	Percentage bond strength of TMT steel (%)	Reference
TMT* steel	2.87	150	20	--	Kute and Wakchaure, 2013
Mild steel	1.79	150	20	62.4	Kute and Wakchaure, 2013
OPBF (6F-028)	1.16	80	30	40.4	This study
Bamboo (*D. giganteus*) with node	1.20	100	19	41.8	Ghavami 1995
Bamboo (*D. giganteus*) without node	0.52	100	19	18.1	Ghavami 1995
Bamboo (*D. asper*)	1.00	200	30	34.8	Muhtar *et al*. 2019
Bamboo (*D. strictus*)	0.73	150	20	25.4	Kute and Wakchaure, 2013
Bamboo (*G. apus*)	0.41	150	12	14.3	Nindyawati and Umniati 2016
Bamboo (*M. bambusoides*)	0.13	100	20	4.4	Agarwal *et al*. 2014

***TMT = thermo-mechanically treated**

588

589 ## 4. Conclusions

590 This study presented results of an experimental investigation into the bond behaviour of OPBF, as
591 single fibres and in combined form as tendons in normal strength concrete at 28, 56 and 112 days. A
592 finite element modelling of bond behaviour between the two materials was also carried out.
593 Consequently, the following conclusions have been made:

594 - Maximum bond strengths of 1.16 MPa, 0.95 MPa and 0.82 MPa were achieved at 28, 56 and
595 112 days respectively;
596 - Average percentage reduction of bond strength at 112 days is 28.4%. This is due to the
597 degradation of OPBF surface in the concrete environment with time;
598 - Bond strength increased with an increase in the number of individual OPBF making up a
599 tendon;
600 - Pre-treatment of OPBF is recommended for cement matrices in order to prevent surface
601 degradation of the fibres by cement alkali;

- Interface bond stress between OPBF and concrete can be modelled using cohesive surface approach in ABAQUS.

Further investigations are required to understand the long-term bond behaviour of OPBF tendons and also OPBF tendons consisting of more than 6 fibres in concrete. Evaluation of improvement methods for the shear resistance between the tendons and concrete is also recommended. The use of OPBF for construction aside being eco-friendly could reduce material importation for developing countries with huge housing deficits.

Acknowledgements

The authors would like to thank the Petroleum Technology Development Fund (PTDF) of Nigeria for sponsoring this research.

Conflict of Interest

None.

References

ABAQUS (2019). Contact formulations for contact pairs in Abaqus/Explicit. See https://abaqus-docs.mit.edu/2017/English/SIMACAEITNRefMap/simaitn-c-expcontactpairform.htm#simaitn-c-expcontactpairform-sliding , Massachusets Institute of Technology, USA. (accessed 29/10/2019).

ACI (American Concrete Institute) (2003) ACI 408R-03: Bond and development of straight reinforcing bars in tension. American Concrete Institute, Farmington Hills, MI, USA.

Agarwal A, Nanda B, and Maity D (2014) Experimental investigation on chemically treated bamboo reinforced concrete beams and columns. Construction and Building Materials **71:** 610-617.

Agopyan A, Savastano HJ, John VM, and Cincotto M A (2005) Developments on vegetable fibre-cement based materials in Sao Paulo, Brazil: an overview. Cement and Concrete Composites **27(5):** 527-536.

Ali A, Lo Conte A, Biffi CA, and Tuissi A (2019) Cohesive surface model for delamination and dynamic behavior of hybrid composite with SMA-GFRP interface. International Journal of Lightweight Materials and Manufacture **2:** 146-155.

Alizadeh V (2019) Finite element analysis of controlled low strength materials. Frontiers of Structural and Civil Engineering **13(5),** 1-8.

ASTM (2016) D4442-16: Standard test methods for direct moisture content measurement of wood and wood-based materials. ASTM International, West Conshohocken, PA, USA.

Ardanuy M, Claramunt J and Filho RDT (2015) Cellulosic fiber reinforced cement-based composites: A review of recent research. Construction and Building Materials **79:** 115-128.

ASTM (2014) C136/C136M-14: Standard test method for sieve analysis of fine and coarse aggregates. ASTM International, West Conshohocken, PA, USA.

Bah EM, Faye I and Geh ZF (2018) The Housing Sector in Africa: Setting the Scene. In: Housing Market Dynamics in Africa. Palgrave Macmillan, London.

Bendetti I and Aliabadi MH (2013) A three-dimensional cohesive-frictional grain-boundary micromechanical model for intergranular degradation and failure in polycrystalline materials. Computer Methods in Applied Mechanics and Engineering, **265:** 36-62.

Blankenhorn PR, Blankenhorn BD, Silsbee MR, and DiCola M (2001) Effects of fiber surface treatments on mechanical properties of wood fiber–cement composites. Cement and Concrete Research **31:** 1049–1055.

Camanho P P and Dávila CG (2002) Mixed-mode decohesion finite elements for the simulation of delamination in composite materials. See https://ntrs.nasa.gov/archive/nasa/casi.ntrs.nasa.gov/20020053651.pdf , NASA, USA. (accessed 29/10/2019)

Campilhoa RDSG, de Moura MFSF and Domingues JJMS (2008) Using a cohesive damage model to predict the tensile behaviour of CFRP single-strap repairs. International Journal of Solids and Structures **45:** 1497–1512.

Campilho RDSG, Banea MD, Pinto AMG, da Silva LFM, and de Jesus AMP (2011) Strength prediction of single-and double-lap joints by standard and extended finite element modelling. International Journal of Adhesion & Adhesives **31:** 363-372.

671 Claramunt J, Lucía F-CJ, Ventura H and Ardanuy M (2016) Natural fiber nonwoven reinforced cement
672 composites as sustainable. Construction and Building Materials **115:** 230-239.

673 Fantilli AP and Vallini P (2007) A cohesive interface model for the pullout of inclined steel fibers in
674 cementitious matrixes. Journal of Advanced Concrete Technology **5(2):** 247-258.

675 Farzad L, Das S and Zhou C (2014) Separation force analysis and prediction based on cohesive
676 element model for constrained-surface Stereolithography processes. Computer-Aided Design **69:**
677 134-142.

678 Ferreira SR, Martinelli E, Pepe M, de Andrade Silva F and Filho RDT (2016) Inverse identification of
679 the bond behavior for jute fibers in cementitious matrix. Composites Part B: Engineering **95:** 440-452.

680 Ferreira SR, Pepe M, Martinelli E, de Andrade Silva F and Filho RDT (2018) Influence of natural
681 fibers characteristics on the interface mechanics with cement based matrices. Composites Part B:
682 Engineering **140:** 183-196.

683 Ganesan N, Indira PV and Himasree PR (2018) Bamboo reinforced concrete wall panels under one
684 way in-plane action. Environment, Development and Sustainability 1-14.

685 Ghavami K (1995) Ultimate load behaviour of bamboo-reinforced lightweight concrete beams.
686 Cement and Concrete Composites **17:** 281-288.

687 Hadi MN (2008) Bond of High Strength Concrete with High Strength Reinforcing Steel. The Open Civil
688 Engineering Journal **2:** 143-147.

689 Hamid B and Abdelmadjid H (2016) Influence of treatments on the date palm fiber and cement matrix
690 behavior: tensile and pull-out tests. American Journal of Civil Engineering and Architecture **4(6):** 211-
691 215.

692 Issa CA and Masri O (2015) Numerical simulation of the bond behavior between concrete and steel
693 reinforcing bars in specialty concrete. International Journal of Civil and Environmental Engineering
694 **9(6):** 767-774.

695 Jendele L and Cervenka J (2006) Finite element modelling of reinforcement with bond. Computers &
696 Structures **84:** 1780-1791.

697 Karade SR (2010) Cement-bonded composites from lignocellulosic wastes. Construction and Building
698 Materials **24(8):** 1323-1330.

699 Khalfallah S and Ouchenane M (2007) A numerical simulation of bond for pull-out tests: the direct
700 problem. Asian Journal of Civil Engineering (Building and Housing) **8(5):** 491-505.

701 Khatun R, Reza MIH, Moniruzzaman M and Yaakob Z (2017) Sustainable oil palm industry: The
702 possibilities. Renewable and Sustainable Energy Reviews **76:** 608-619.

703 Kute SY and Wakchaure MR (2013) Performance evaluation for enhancement of some of the
704 engineering properties of bamboo as reinforcement in concrete. Journal of The Institution of
705 Engineers (India): Series A **94(4):** 235-242.

706 Machaka M, Basha H, Chakra HA and Elkordi A (2014) Alkali treatment of fan palm natural fibers for
707 use in fiber reinforced concrete. European Scientific Journal **10(12):** 186-195.

708 Mali PR. and Datta D (2018) Experimental evaluation of bamboo reinforced concrete slab panels.
709 Construction and Building Materials **188:** 1092-1100.

Mali PR and Datta D (2019) Experimental study on improving bamboo concrete bond strength. Advances in concrete construction **7(3):** 191-201.

Momoh EO and Dahunsi BIO (2017) Suitability of oil-palm-broom-fibres as reinforcement for laterite-based roof tiles. International Journal of Software & Hardware Research in Engineering **5(4):** 27-35.

Momoh EO and Osofero AI (2019). Behaviour of oil palm broom fibres (OPBF) reinforced concrete. Construction and Building Materials, **221:** 745-761.

Momoh EO and Osofero AI (2020). Recent developments in the application of oil palm fibres in cement composites. Frontiers of Structural and Civil Engineering. https://doi.org/10.1007/s11709-019-0576-9.

Momoh EO, Osofero AI, Martinez-felipe A and Hamza F (2020) Physico-mechanical behaviour of Oil Palm Broom Fibres (OPBF) as eco-friendly building material. Journal of Building Engineering **30:** 101208.

Morrissey FE, Coutts RSP and Grossman PUA (1985) Bond between cellulose fibres and cement. International Journal of Cement Composites and Lightweight Concrete **7(2):** 73-80.

Muhtar M, Dewi SM and Munawir A (2019) Enhancing bamboo reinforcement using a hose-clamp to increase bond-stress and slip resistance. Journal of Building Engineering **26:** 100896.

Naik DL, Sharma A, Chada RR, Kiran R and Sirotiak T (2019) Modified pullout test for indirect characterization of natural fiber and cementitious matrix interface properties. Construction and Building Materials **208:** 381-393.

Nindyawati N and Umniati BS (2016) Bond strength of bamboo reinforcement in light weight concrete. Journal of Civil Engineering and Architecture **10:** 417-420.

Omar FN, Mohammed MAP and Baharuddin AS (2014) Effect of silica bodies on the mechanical behaviour of oil palm empty fruit bunch fibres. BioResources **9(4):** 7041-7058.

Onuaguluchi O and Banthia N (2016) Plant-based natural fibre reinforced concrete composites: a review. Cement and Concrete Composites, **68:** 96-108.

Osofero AI, Corradi M and Borri A (2015) Experimental study of bond strength between titanium bar and lime-based mortar. Journal of Materials in Civil Engineering **27(6):** 1-10.

Pacheco-Torgal F and Jalali S (2010) Cementitious building materials reinforced with vegetable fibres: A review. Construction and Building Materials. https://doi.org/10.1016/j.conbuildmat.2010.07.024

Pacheco-Torgal F and Jalali S (2011) Natural fiber reinforced concrete. In: Fibrous and Composite Materials for civil Engineering Applications (Ed: R. Fangueiro). Woodhead Publishing. Pp. 154-167. https://doi.org/10.1533/9780857095583.2.154

Page J, Khadraoui F, Boutouil M and Gomina M (2017) Multi-physical properties of a structural concrete incorporating short flax fibers. Construction and Building Materials, **140:** 344-353.

Pereira H, Cunha V and Sena-Cruz J (2015) Numerical simulation of galvanized rebars pullout. Frattura ed Integrità Strutturale **31:** 54-66.

Ramakrishna G and Priyadharshini S (2018) Effect of embedment length of untreated natural fibres on the bond behaviour in cement mortar. Frontiers of Structural and Civil Engineering **12(4):** 454-460.

Ramakrishna G and Sundararajan T (2005) Impact strength of a few natural fibre reinforced cement mortar slabs: a comparative study. Cement and Concrete Composites, **27(5):** 547-553.

Ramamurthi M, Lee J-S, Yang S-H and Kim Y-S (2013) Delamination characterization of bonded interface in polymer coated steel using surface based cohesive model. International Journal of Precision Engineering and Manufacturing **14(10):** 1755-1765.

Sakaray H, Togati NVVK and Reddy IVR (2012) Investigation on properties of bamboo as reinforcing material in concrete. International Journal of Engineering Research and Applications (IJERA) **2(1):** 77-83.

Savastano Jr H and Agopyan V (1999) Transition zone studies of vegetable fibre-cement paste composites. Cement and Concrete Composites **21:** 49-57.

Seixas MA, Ripper LA and Ghavami K (2014) Deployable bamboo structure for sustainable architecture. In *Proceedings of the 15th International Conference on Non-Conventional Materials and Technologies*, Pirassununga, Brazil, pp. 23-25.

Serpieri R, Alfano G and Sacco E (2015) A mixed-mode cohesive-zone model accounting for finite dilation and asperity degradation. International Journal of Solids and Structures **67-68:** 102-115.

Silva FA, Mobasher B, Soranakom C and Filho RDT (2011) Effect of fiber shape and morphology on interfacial bond and cracking behaviors of sisal fiber cement based composites. Cement & Concrete Composites **33:** 814-823.

Singh P and Scanlon A (2013) Concrete in Residential Construction. Housing Research Center, Pennsylvania, USA.

Singh S, Shukla A and Brown R (2004) Pullout behavior of polypropylene fibers from cementitious matrix. Cement and Concrete Research **34:** 1919-1925.

Soulioti DV, Barkoula N-M, Koutsianopoulos F, Charalambakis N and Matikas TE (2013) The effect of fibre chemical treatment on the steel fibre/cementitious matrix interface. Construction and Building Materials **40:** 77-83.

Sun CT and Jin Z-H (2012) Cohesive Zone Model. In *Fracture Mechanics.* Elsevier, ISBN: 978-0-12-385001-0 pp. 227-246.

Wan KT and Parris J (2016) Investigation of natural fibre reinforced cementitious composite for structural retrofitting of building structures. In *International Association for Bridge and Structural Engineering (IABSE) Symposium Report*, Stockholm, Sweden, 106(7), pp. 623-629.

Wei J and Meyer C (2014) Improving degradation resistance of sisal fiber in concrete through fiber surface treatment. Applied Surface Science **289:** 511-523.

Wei J and Meyer C (2015) Degradation mechanisms of natural fiber in the matrix of cement composites. Cement and Concrete Research **73:** 1-16.

Zenon A and Pilakoutas K (2004) Bond behavior of fiber reinforced polymer bars under direct pullout conditions. Journal of Composites for Construction **8(2):** 173-181.

Bond Behaviour of Oil Palm Broom Fibres in Concrete for Eco-friendly Construction

Momoh, Emmanuel Owoichoechi [1] Osofero, Adelaja Israel [2] Menshykov, Oleksandr[3]
School of Engineering, University of Aberdeen, King's College, Aberdeen, AB24 3UE, United Kingdom[1,2,3]
r01eom18@abdn.ac.uk[1], aiosofero@abdn.ac.uk[2], o.menshykov@abdn.ac.uk [3]

Figures

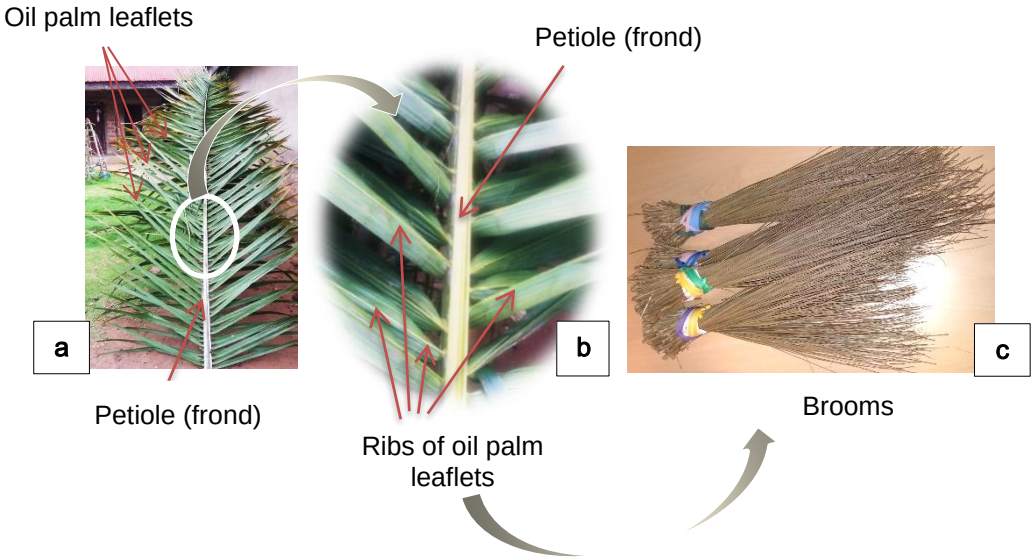

Figure 1.1: Illustration of OPBF: (a) oil palm leaf; (b) magnified image of oil palm leaf; (c) OPBF tied into broom units (Momoh and Osofero 2020)

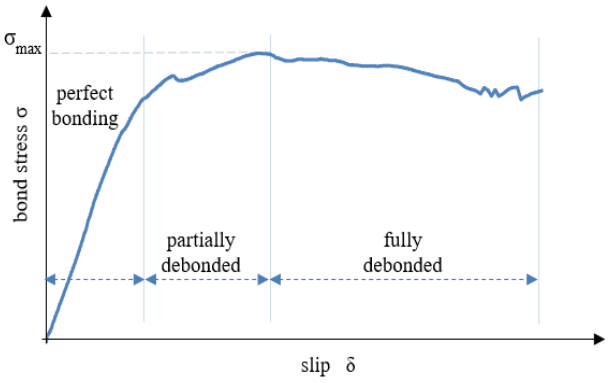

Figure 1.2: Typical stress-displacement curve of pull-out of a single OPBF from concrete

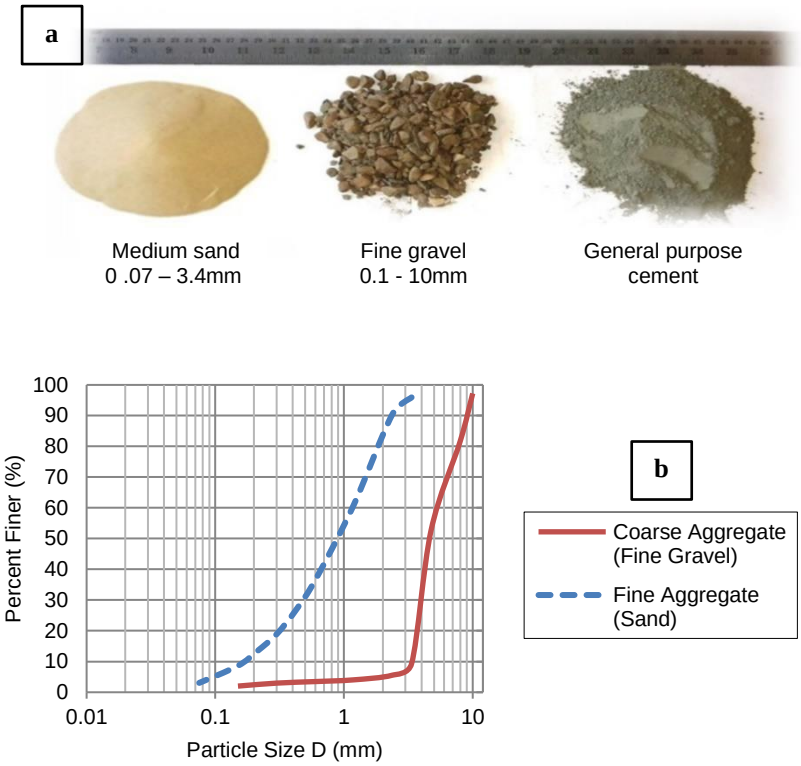

Figure 2.1: (a) Constituents of concrete; (b) Grading curves of fine and coarse aggregates

799

Figure 2.2: Illustration of OPBF tendons consisting of (from left to right) 2, 3, 4, 5 and 6 fibres per tendon respectively

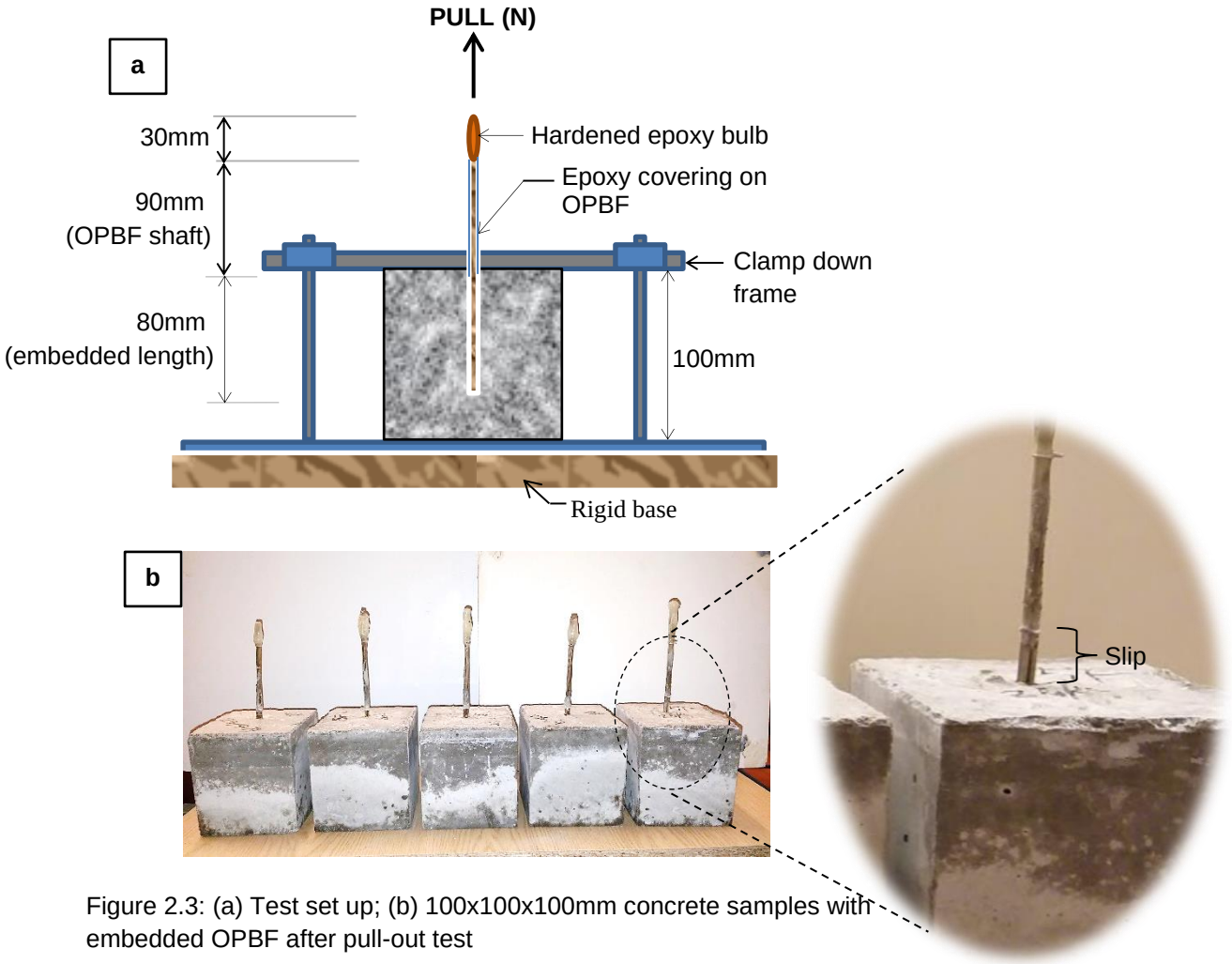

Figure 2.3: (a) Test set up; (b) 100x100x100mm concrete samples with embedded OPBF after pull-out test

800

Figure 2.4: Curing of samples

801

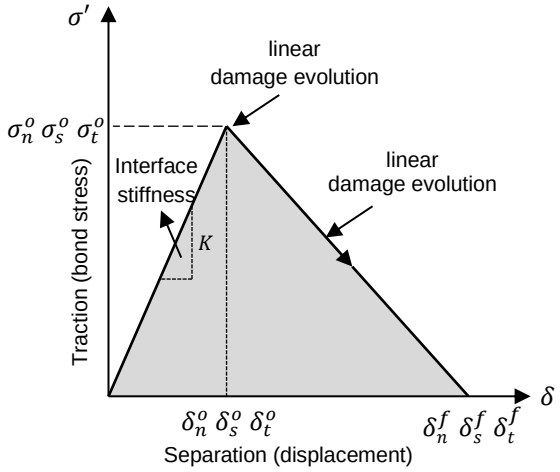

Figure 2.5: Traction-separation response

826

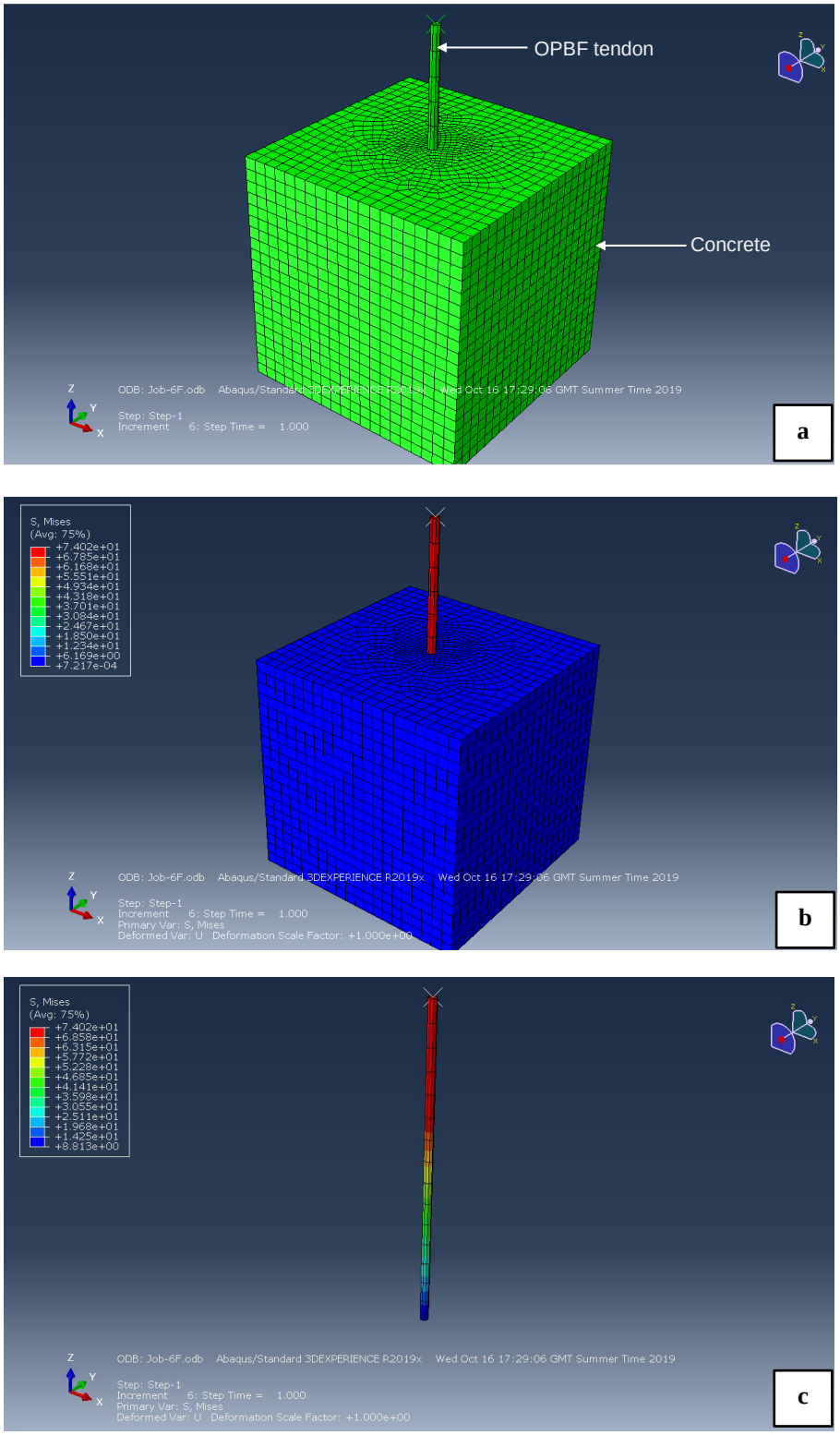

Figure 2.6: (a) Meshing arrangement of model; (b) Stress distribution at the end of simulation; (c) Stress distribution on a model of OPBF tendon

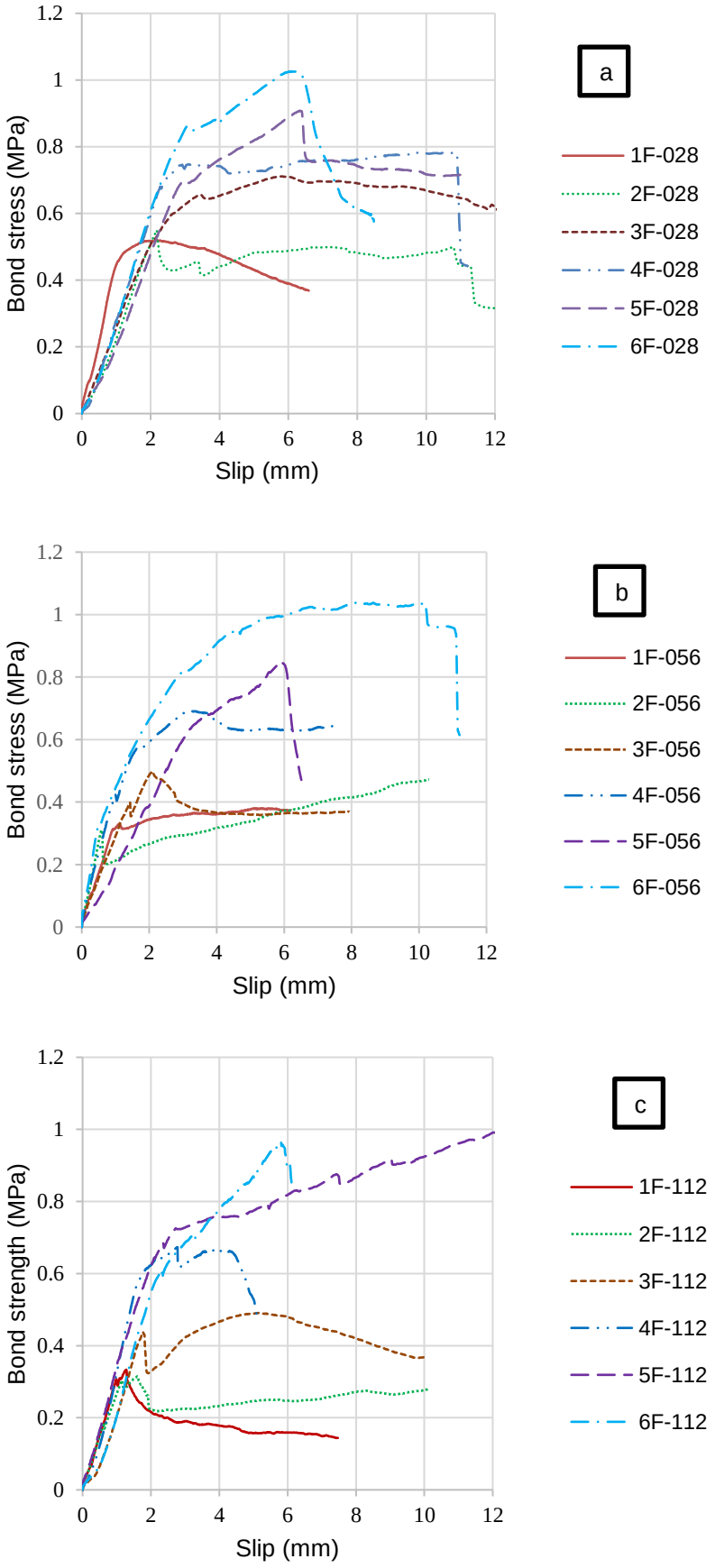

Figure 3.1: Bond stress curves at; (a) 28, (b) 56 and (c) 112 days

827

Figure 3.2: Illustration of damage to OPBF after complete pull-out at 112 days

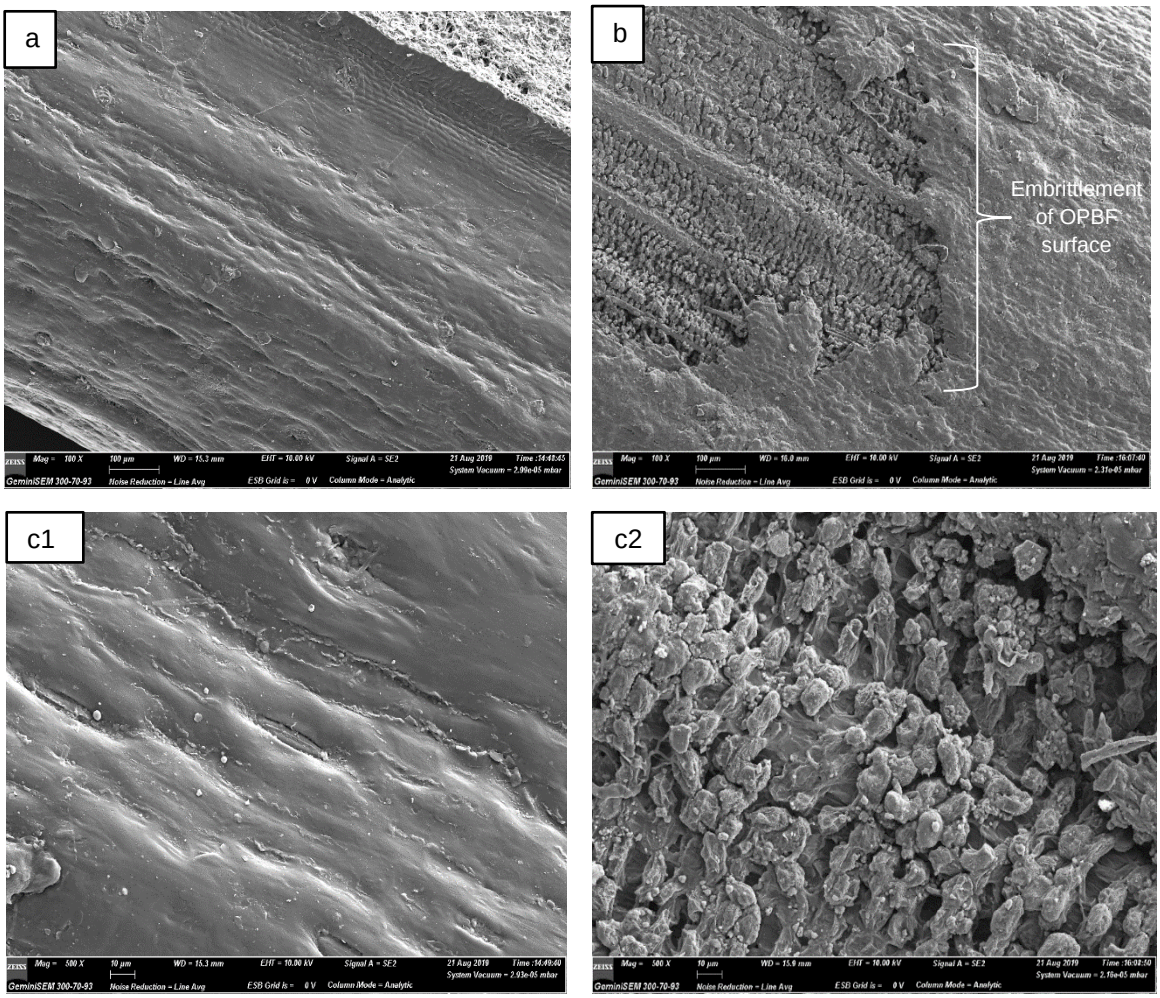

Fig 3.3: Scanning Electron Microscopy of OPBF surfaces:
(a) Before inserting in concrete x100;
(b) 112 days of inserting in concrete x100;
(c1) Unembrittled surface of OPBF x500;
(c2) Embrittled surface of OPBF x500.

838

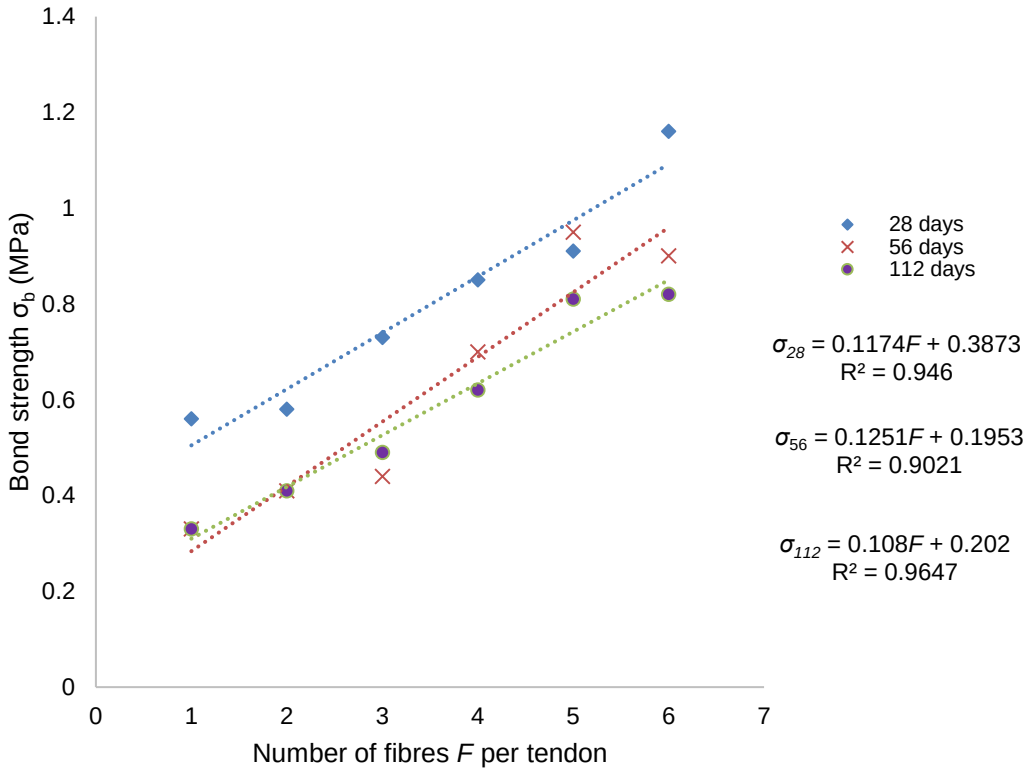

Figure 3.4: Linear models of bond stress between concrete and OPBF at 28, 56 and 112 days

839

840

841

842

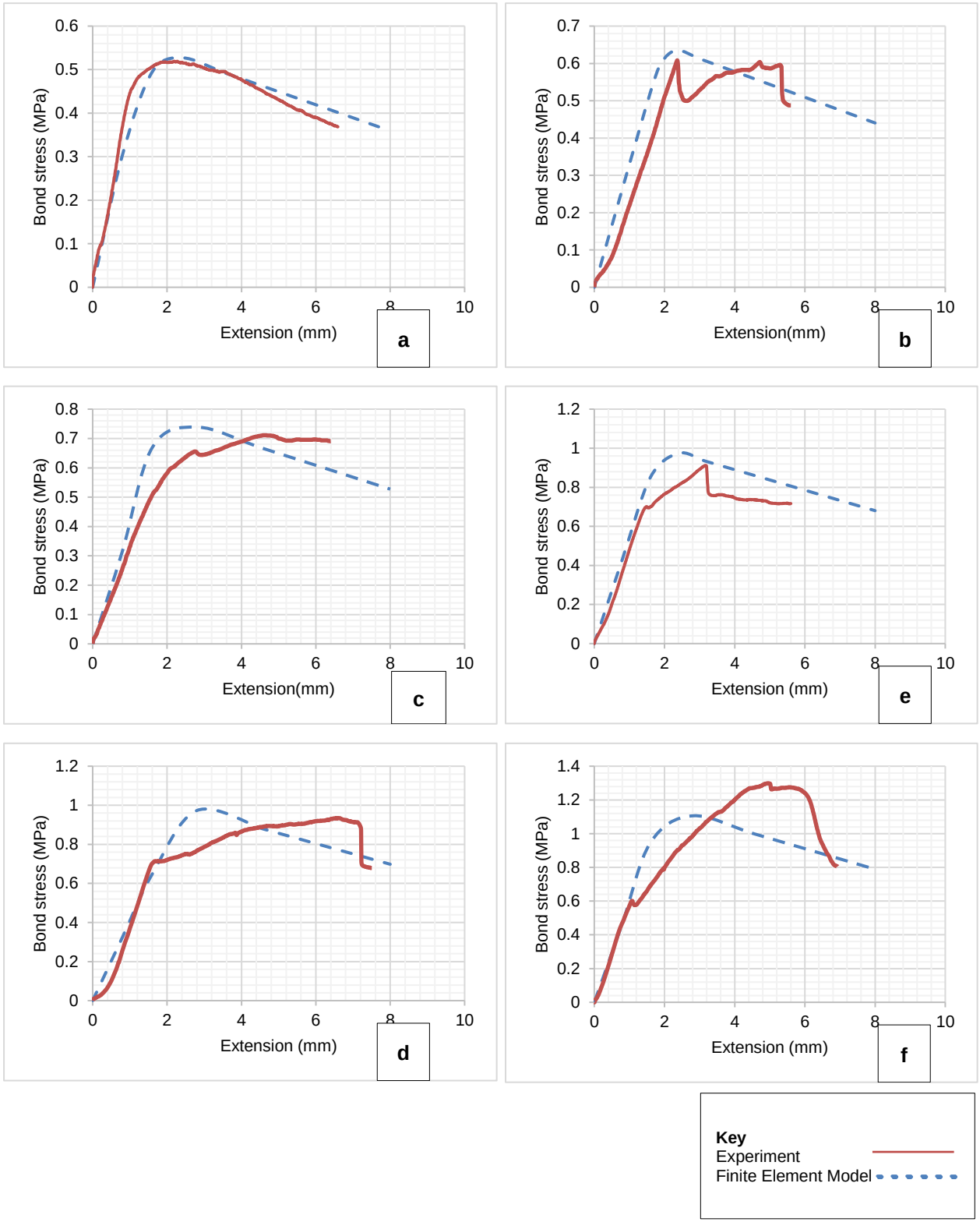

Figure 3.5: Bond (pull-out) stress behaviour between OPBF and concrete
(a) 1 fibre/tendon (b) 2 fibres/tendon (c) 3 fibres/tendon (d) 4 fibres/tendon (e) 5 fibres/tendon (f) 6 fibres/tendon

843